Available online at www.sciencedirect.com
SCIENCE DIRECT®
Journal of Solid State Chemistry 177 (2004) 2432–2439
JOURNAL OF SOLID STATE CHEMISTRY
http://elsevier.com/locate/jssc

Local order structure and surface acidity properties of a Nb_2O_5/SiO_2 mixed oxide prepared by the sol–gel processing method

Maria Suzana P. Francisco,[a,*] Richard Landers,[b] and Yoshitaka Gushikem[a]

[a] Departamento de Inorgnica, Instituto de Química, Universidade Estadual de Campinas, P.O. Box 6154, 13084-971 Campinas SP, Brazil
[b] Instituto de Física Gleb Wataghin, Universidade Estadual de Campinas, P.O. Box 6165, 13084-971 Campinas SP, Brazil

Received 16 December 2003; received in revised form 23 March 2004; accepted 28 March 2004

Abstract

The sol–gel processing method was used as an alternative route to obtain Nb_2O_5 phase homogenously dispersed in the SiO_2 matrix, improving the thermal stability of the Brønsted acid sites, Nb–OH and Nb–OH–Si groups. The local niobium structure and the influence of the amount of niobia on the surface of the Nb_2O_5/SiO_2 system were studied by XAS and XPS, respectively. For the samples calcined at 423 and 873 K, the $3d_{5/2}$ BE values are at ca. 208.2 eV, indicating an ionic character for Nb(V) species in the SiO_2 matrix, probably associated to Si–O–Nb linkages. The features of Nb K-edge XANES spectra of samples show the absence of Nb=O species. The Nb K-edge EXAFS oscillations exhibit a shoulder at ca. 5.6 $Å^{-1}$, which probably arises from Nb–O–Si. This fact corroborates the EXAFS simulation data of the second coordination shell, whose best fitting is achieved with three distances, two Nb–Nb lengths and one Nb–Si.
© 2004 Elsevier Inc. All rights reserved.

Keywords: Niobia supported in silica; Sol–gel processing method; XAS; XPS; Acid sites

1. Introduction

Many catalytic applications for a highly dispersed Nb_2O_5 phase on the SiO_2 surface, obtained by the grafting process, have been described [1–9]. The preparations procedures consist in reacting a precursor reagent of the metal oxide with the ≡SiOH group on the SiO_2 surface and formation of a monolayer film adhered onto a substrate surfaces by means of Si–O–Nb bond formation [10–12]. The Lewis and Brønsted acid densities on the surface have been monitored by controlling the amount and degree of dispersion of the metal oxides adhered onto the surface since such characteristics may have a great influence on the catalytic performance of these materials [13–15].

As an alternative procedure, the sol–gel processing method has been used to homogeneously disperse Nb_2O_5 phase in the SiO_2 matrix [16]. In this case niobium oxide, different from what is found adhered on a silica matrix obtained by the grafting method, is dispersed in the bulk of the SiO_2 matrix as aggregated nanosized particles. In this way, the Nb_2O_5 particles are confined inside the SiO_2 matrix conferring low mobility to them, even upon heating the mixed oxide solid at high temperatures [17]. Therefore, the local structure for Nb_2O_5 obtained by the sol–gel processing method can be different, when compared with the bidimensional oxide monolayer obtained by the grafting process.

The Nb_2O_5 particles in the sol–gel matrix, as revealed by transmission electron microscopy [17], show a phase transition depending on the amount of the metal oxide present in the matrix, becoming crystalline upon heating above 1000 K, while the SiO_2 matrix remains amorphous even when heating at temperatures as high as ca. 1473 K.

Therefore, for a solid obtained by the sol–gel processing method, a more detailed investigation to characterize such systems as obtained is required since the observed acid properties depend on the local niobium oxide structure. Aiming to obtain such information in the present work, the dynamics of the structural changes of the Nb_2O_5/SiO_2 system were obtained using X-ray photoelectron spectroscopy

*Corresponding author. Fax: +55-19-3788-3023.
E-mail address: suzana@iqm.unicamp.br (M.S.P. Francisco).

0022-4596/$ - see front matter © 2004 Elsevier Inc. All rights reserved.
doi:10.1016/j.jssc.2004.03.035

(XPS) and X-ray absorption spectroscopy (XAS). The nature of the acid sites was investigated by Fourier transform infrared (FT-IR spectroscopy) with pyridine as molecular probe. The overall findings are then correlated with the thermal stability of the Lewis and Brønsted acid sites. The results were obtained for different niobium oxide amounts in the silica and for different treatment temperatures.

2. Experimental

2.1. Samples preparations

The sol–gel method was employed to prepare Nb_2O_5/SiO_2 samples according to the following procedure [17]. Tetraethylorthosilicate (TEOS, Aldrich) was mixed with dry ethanol in the molar proportion TEOS : EtOH = 1 : 3.8. To 50 cm^3 of this solution, 0.86 cm^3 of concentrated HCl solution was added and then the solution was refluxed for 2.5 h. The resulting solution is designated as solution A. Another solution, called B, was prepared by dissolving high purity solid $NbCl_5$ (from Companhia Brasileira de Metalurgia e Mineração, CBMM) in 50 cm^3 of dry ethanol (concentrations 0.22, 0.45, and 0.67 mol L^{-1}). These solutions were allowed to react under a N_2 atmosphere until production of gaseous HCl was not detected. At this stage, practically all Nb is in the $Nb(OEt)_5$ form. Solution B was added to solution A and the mixtures were stirred at room temperature for 3 h. After this time, 140 cm^3 of H_2O was slowly added to the mixture followed by stirring at room temperature for 2 h. Finally, the mixture was allowed to rest at 333 K until complete gelation. The solids were washed several times with water and finally with dry ethanol. The residual solvent from the xerogels was evaporated at 383 K for 24 h, and the solid materials were ground and sieved to 200 mesh. The final materials Nb_2O_5/SiO_2 (2.5, 5.0, and 7.5 as Nb_2O_5 mol percentage with respect to silica) were calcined in the temperature range between 423 and 1273 K.

The powdered samples thus prepared were designated as 2.5% Nb_2O_5/SiO_2, 5.0% Nb_2O_5/SiO_2, and 7.5% Nb_2O_5/SiO_2. Commercial amorphous SiO_2 (Fluka) and Nb_2O_5 (CBMM) were used in specific investigations.

2.2. XPS study

The XPS analysis was performed using a VSW HA-100 Spherical Analyzer, with an Al ($K\alpha$ line, $hv = 1486.6$ eV) X-ray source. The high-resolution spectra were measured with constant analyzer pass energy of 44 eV, which produces a FWHM line width of 1.8 eV for the Au $4f_{7/2}$ line. The powdered samples were pressed into pellets and fixed to a stainless steel sample holder with double-faced tape and analyzed without further preparation. The binding energies were referenced to an adventitious C 1*s* line at 284.6 eV. Prior to curve fitting with Gaussian line shapes, a linear background was subtracted from the data. The atomic compositions were obtained from the C 1*s*, O 1*s*, Si 2*p*, and Nb 3*d* peak areas, using cross sections for photo-ionization from the literature [18].

2.3. XAS analyses

The XAS measurements at room temperature were done at XAFS beam line of National Synchrotron Light Laboratory (LNLS) in Campinas (ring energy of 1.37 GeV and beam current about 175 mA). The X-ray absorption near-edge spectroscopy (XANES) and X-ray absorption fine structure (EXAFS) spectra for the calcined samples were obtained and, for comparison, the spectrum for amorphous niobia was also acquired.

The monochromator was double crystal Si (220) and the incident and transmitted photon intensities were determined by means of standard ion chamber detectors. The energy steps were 0.8 eV for the XANES region. For the EXAFS region, five scans were acquired for each sample with steps of 2.0 eV. The energy ranges were 18,920–19,250 and 18,920–19,600 eV for XANES and EXAFS regions, respectively. The EXAFS data analyses were done by a standard procedure of data reduction, using the computational program CDXAS [19]. The curve-fitting analysis was performed by using theoretical phase shifts and amplitude functions from the simple pair Nb–O, and from Nb foil (ICSD file 76554) [20] and $NbSi_2$ (ICSD file 16502) [21], which were calculated by the FEFF7.0 computational program.

2.4. Infrared spectroscopy study

The Lewis and Brønsted acid sites of the pre-calcined samples (383 K) were investigated after pyridine adsorption for 15 min, with subsequent drying under low pressure ($\sim 10^{-5}$ Pa for 30 min) at different temperatures (298–523 K). The Fourier transform infrared spectra (FT-IR) were obtained as pressed disks in the range of 1650–1400 cm^{-1}, using a Bomem MB-Series instrument. For comparison, the FT-IR spectra of pyridine adsorbed on a silica surface were acquired following the same procedure as described above.

3. Results and discussion

3.1. XPS analyses

Nb 3*d* X-ray photoelectron spectra for 2.5% Nb_2O_5/SiO_2, 5.0% Nb_2O_5/SiO_2, and 7.5% Nb_2O_5/SiO_2 samples, calcined at 423, 873, and 1273 K, are presented in

Fig. 1. Table 1 lists the corresponding binding energy (BE values) and the Nb/Si atomic percentage.

The O 1*s* BE peaks at 532.8 and 531.0 eV, for oxygen bonded to Si and Nb atoms, respectively, do not change with the thermal treatment and with the different compositions of the Nb_2O_5/SiO_2 system. The first value obtained is the same observed for O 1*s* bulk phase in SiO_2 gel and the second one in Nb_2O_5 [22–25]. Similarly, Si 2*p* BE peak values, observed at 103.6 eV, are the same for the three compositions and after the thermal treatments [24,25].

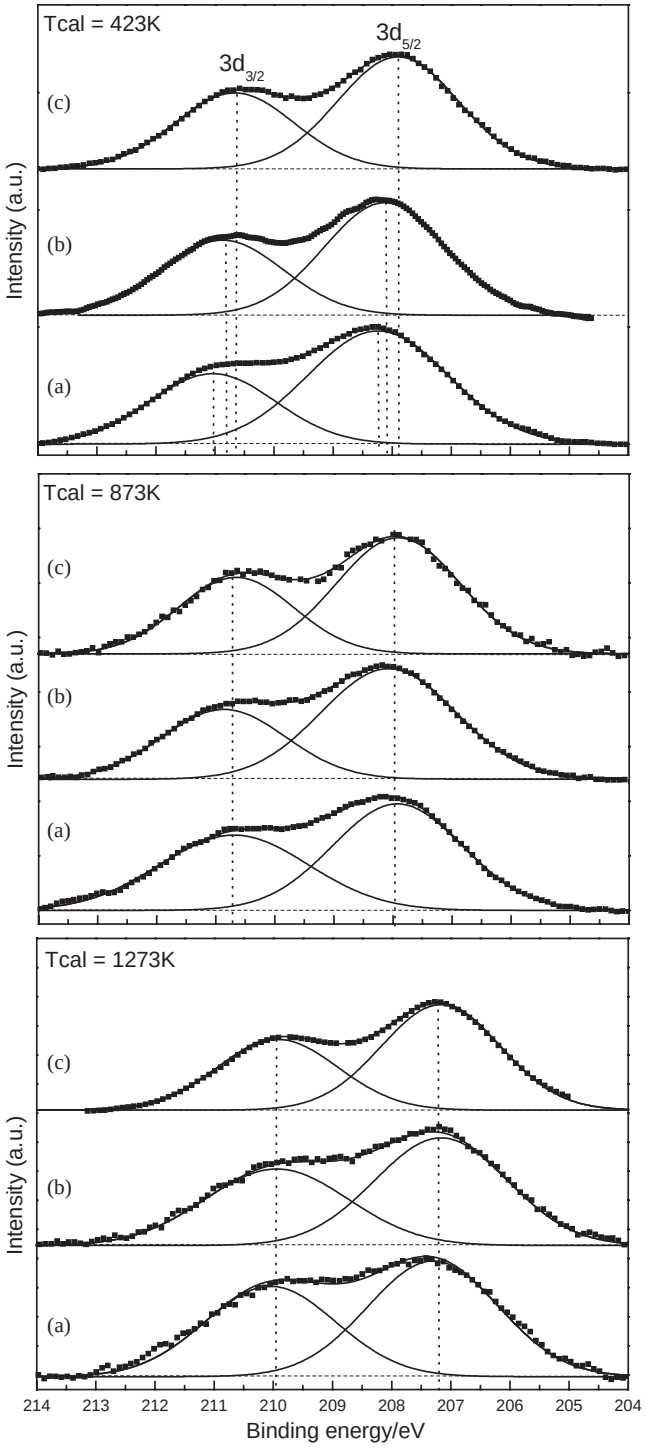

Fig. 1. Nb 3*d* X-ray photoelectron spectra recorded for the: (a) 2.5% Nb_2O_5/SiO_2; (b) 5.0% Nb_2O_5/SiO_2; and (c) 7.5% Nb_2O_5/SiO_2 samples calcined at 423, 873, and 1273 K.

Table 1
XPS BE values as a function of Nb-content and temperature of thermal treatment for the Nb_2O_5/SiO_2 system and Nb/Si atomic percentage

Samples	BE (eV)				Nb/Si (at%)
	Nb $3d_{5/2}$	Si 2*p*	O 1*s*		
			Si–O	Nb–O	
$T = 423$ K					
2.5% Nb_2O_5/SiO_2	208.5 (2.4)[a]	103.6 (2.5)	532.9	531.0	3
5.0% Nb_2O_5/SiO_2	208.3 (2.6)	103.5 (2.5)	532.8	530.9	6
7.5% Nb_2O_5/SiO_2	208.0 (2.4)	103.4 (2.4)	532.8	531.0	8
$T = 873$ K					
2.5% Nb_2O_5/SiO_2	208.0 (2.7)	103.4 (2.5)	532.7	531.0	3
5.0% Nb_2O_5/SiO_2	208.3 (2.6)	103.6 (2.5)	532.6	530.9	7
7.5% Nb_2O_5/SiO_2	208.0 (2.3)	103.6 (2.3)	532.9	531.0	7
$T = 1273$ K					
2.5% Nb_2O_5/SiO_2	207.6 (2.8)	103.7 (2.5)	532.8	531.0	3
5.0% Nb_2O_5/SiO_2	207.3 (2.4)	103.5 (2.5)	532.9	531.1	3
7.5% Nb_2O_5/SiO_2	207.7 (2.4)	103.7 (2.5)	532.7	530.8	4

[a] (FWHM) = full-width at half-maximum.

The two spin–orbit components, Nb $3d_{5/2}$ and $3d_{3/2}$ BE peaks, change depending on the thermal treatment of the samples. For the samples calcined at 423 and 873 K, the $3d_{5/2}$ BE values remain practically unchanged at ca. 208.2 eV. After heating the samples at 1273 K, the BE peaks shift to a lower energy region, i.e., ca. 207.5 eV. This value is the same as that exhibited by bulk Nb_2O_5, where $3d_{5/2}$ BE is observed at 207.5 eV with multiplet splitting of 2.5 eV [26–29]. The BE shift is associated with a decrease of the Nb atom ionic character upon heat treatment. This behavior can be explained by taking into consideration that the niobium atoms are highly dispersed in the matrices and attached to the silica by Si–O–Nb bonding, whose origin occurred during the condensation process of the sol–gel matrix [30]. Upon the higher temperature, 1273 K, the metal oxides segregate and agglomerate into larger particles, with breaking of Si–O–Nb bonds, and the observed BE is that of bulk phase Nb_2O_5 calcined at 1273 K [31]. The ionic character of Nb atoms in the Nb_2O_5/SiO_2 system calcined at lower temperatures is similar to the atoms in $NbCl_5$, whose $3d_{5/2}$ BE value is 208.2 eV [29].

Table 1 shows the Nb/Si atomic percentage probed by the XPS technique. The amount of the Nb atoms on the surface does not change significantly for samples heated up to 873 K, indicating that the oxide particles are not thermally mobile. This behavior is a consequence of the highly and well-dispersed character of the niobia species

in the SiO_2 matrix. For samples calcined at 1273 K, the metal amount on the surface showed a significant decrease. This fact can be noted by the observation of the Nb/Si atomic ratios that decrease from 6% to 3% for 5.0% Nb_2O_5/SiO_2 sample and from 8% to 4% for 7.5% Nb_2O_5/SiO_2 sample. For 2.5% Nb_2O_5/SiO_2 sample, the Nb/Si ratio does not change because, in this case, the niobium oxide particles are much more dispersed and the crystalline particle sizes are also much smaller. It must be remembered that SiO_2 in every case remained amorphous, as was shown by XRD and transmission electron microscopy images [17].

3.2. XAS analyses

The Nb K-edge XAS spectra and the corresponding structural parameters for 2.5% Nb_2O_5/SiO_2, taken as a representative sample, were obtained. Fig. 2 presents the Nb K-edge XANES spectra obtained for samples calcined at 423, 573, and 873 K, and for pure Nb_2O_5 as reference (amorphous phase).

Independent of the thermal treatment, the niobium species in the samples and in the reference exhibit very similar XANES features: a not well-defined pre-edge adsorption and two peaks in the post-edge region. The pre-edge peak is due to the $s-d$ transitions and the intensity depends on the coordination, being low for octahedral [16]. Some authors have assumed that the absence of this peak is attributed to the lack of a Nb=O bond on the silica surface, which is due to tetracoordinated niobia species [16,32] or, as is known for heavy elements like niobium, sometimes the internal transitions responsible for the peaks in the pre-edge are so weak that they do not appear clearly in the XANES spectrum.

Fig. 3(A) presents the Nb K-edge EXAFS spectra of the samples calcined at 423, 573, and 873 K, and of pure

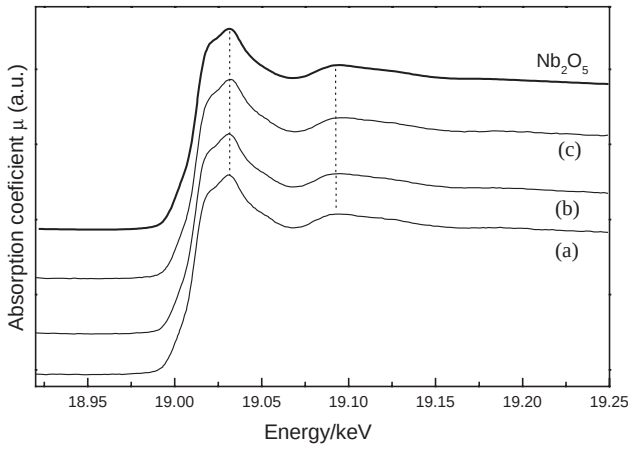

Fig. 2. Nb K-edge XANES spectra from 2.5% Nb_2O_5/SiO_2 samples calcined at: (a) 423 K, (b) 573 K, and (c) 873 K, and from pure Nb_2O_5 (amorphous phase).

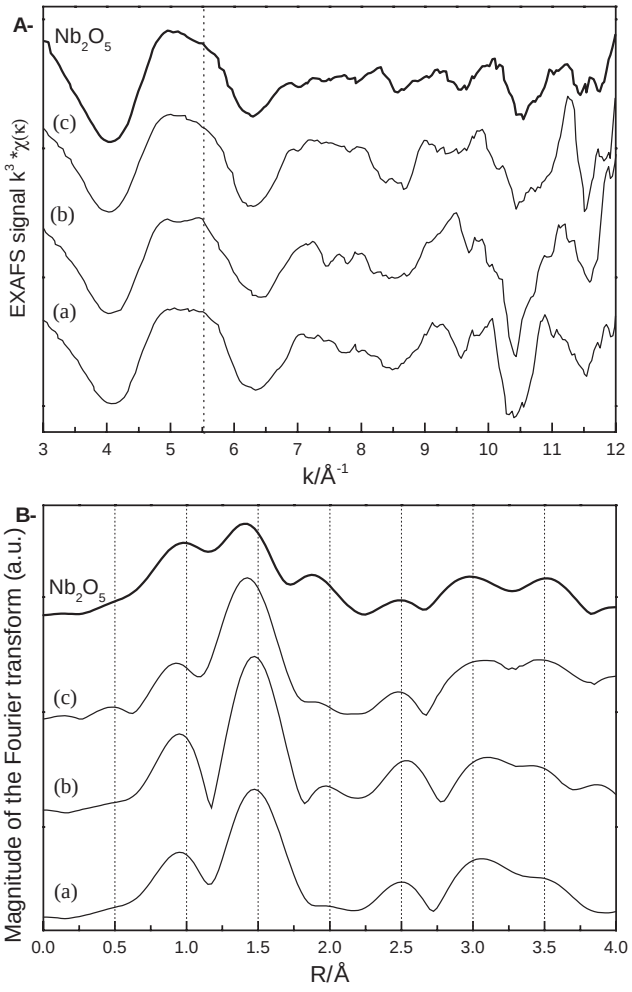

Fig. 3. Nb K-edge EXAFS spectra (A) from 2.5% Nb_2O_5/SiO_2 sample calcined at (a) 423 K, (b) 573 K, and (c) 873 K, and from the pure Nb_2O_5 (amorphous phase), and the respective Fourier transforms of the Nb K-edge EXAFS (B) in the k range of 3.00–12.00 $Å^{-1}$.

Nb_2O_5. The EXAFS oscillations of the sample, calcined at different temperatures, exhibit a shoulder at ca. 5.6 $Å^{-1}$ when compared to the pure Nb_2O_5 spectrum, this peak is attributed to the interference of the backscattered electron wave by the silicon atom at ca. 3.30 Å [33].

The magnitudes of the Fourier transforms of Nb K-edge EXAFS spectra (denoted as $|F(r)|$) in the k range of 3.00–12.00 $Å^{-1}$ for the sample calcined at 423, 573, and 873 K, and for pure Nb_2O_5 (amorphous phase) are presented in Fig. 3(B). The static disorder of the oxygen around the niobium is responsible for the rapid fall to low frequency EXAFS oscillations, creating beats that lower the amplitude of the total signal, together with a broad low-r peak in the Fourier transform for crystallite Nb_2O_5 and Nb_2O_5 dispersed in glass [34,35].

For niobia in the H crystallographic phase, the Nb–O first neighbor bond lengths are found around three values, 1.82, 1.97 and 2.24 Å, with average coordination

numbers 1.6, 3.0 and 1.2, respectively [33,36]. As a consequence of this large range of Nb–O distance distributions (low crystalline symmetry of Nb_2O_5), the interference of the backscattered electron waves has a highly destructive degree, leading to more non-defined peaks in the $|F(r)|$ for the corresponding region [34]. For this reason the $|F(r)|$ in the region related to the peaks of first neighbor backscattering (0.5–2.2 Å), for both the sample and the reference compound, is less structured.

The distances, the coordination numbers and the Debye–Waller factors (denoted R, N, and σ, respectively) of the first coordination shell Nb–O (distances between 0.5 and 2.2 Å) were determined by curve-fitting analyses for the samples calcined at 423, 573, and 873 K (see Table 2), Fig. 4(A) presents experimental (dot) and simulated (solid line) curves. A simple Nb–O pair was taken to achieve the theoretical phase shift and amplitude function to simulate the EXAFS data, making use of the FEFF7.0 computational program.

The best-fit results for the first coordination shell were obtained taking in consideration the presence of three distances (types of Nb–O bond) for both the sample (independent of its thermal treatment) and for pure Nb_2O_5 (see Table 2). No difference in the structural parameters for the sample calcined at different temperatures can be noted and the lengths of the Nb–O bonds and their, respectively, coordination numbers do not change substantially.

The comparison between the structural parameters obtained for pure Nb_2O_5 and those obtained for the sample shows some differences in the Nb–O bond distances: all three Nb–O bond lengths are longer for pure Nb_2O_5, 1.76, 1.98, and 2.25 Å, and the respective coordination numbers, 2.4, 3.2 and 0.6, sum to 6. We also can note that the corresponding Debye–Waller factors are higher for pure Nb_2O_5, suggesting a higher disorder of the local structure of non-supported Nb_2O_5 than that for the 2.5% Nb_2O_5/SiO_2 sample.

For the second niobium coordination shell (distances between 2.7 and 3.8 Å), in the $|F(r)|$ of pure Nb_2O_5 it is possible to distinguish two peaks centered at ca. 3.0 and 3.5 Å. These peaks are due to the backscattering of niobium (second neighbor). For the samples calcined at

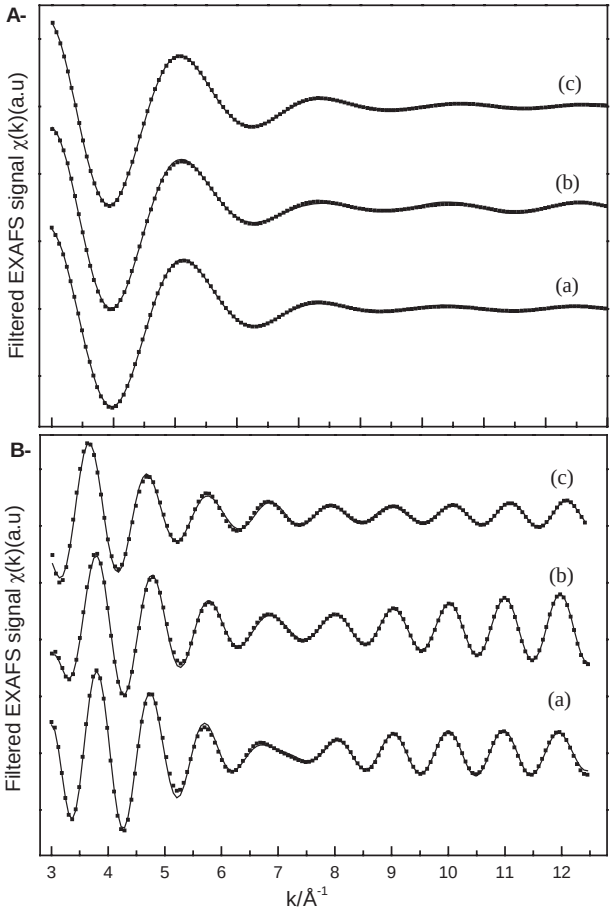

Fig. 4. Comparison between the filtered signal (line) and the related fit (dot) for 2.5% Nb_2O_5/SiO_2 samples calcined at (a) 423 K, (b) 573 K, and (c) 873 K: (A) first coordination shell (Nb–O) and (B) second coordination shell (Nb–Nb).

Table 2
Curve fitting analyses of Fourier transforms of Nb K-edge EXAFS data for the 2.5% Nb_2O_5/SiO_2 sample calcined at 423, 573, and 873 K and for reference Nb_2O_5

T (K)	Nb–O			Nb–O			Nb–O		
	N (±0.3)	R (Å) (±0.03)	σ (Å) (±0.02)	N (±0.3)	R (Å) (±0.03)	σ (Å) (±0.02)	N (±0.3)	R (Å) (±0.03)	σ (Å) (±0.02)
423	1.0	1.69	0.08	2.1	1.93	0.03	0.5	2.17	0.06
573	1.2	1.69	0.03	2.1	1.88	0.06	1.1	2.10	0.06
873	1.4	1.70	0.09	2.3	1.90	0.07	0.5	2.18	0.05
Nb_2O_5	2.4	1.76	0.14	3.2	1.98	0.16	0.6	2.25	0.07
	Nb–Nb			Nb–Si			Nb–Nb		
423	1.0	3.16	0.12	1.0	3.39	0.08	2.1	3.72	0.10
573	1.4	3.24	0.13	1.0	3.39	0.09	2.5	3.76	0.07
873	1.3	3.26	0.16	1.4	3.37	0.07	3.0	3.69	0.08
Nb_2O_5	1.8	3.19	0.11	—	—	—	4.3	3.85	0.12

different temperatures, the $|F(r)|$ present peaks at ca. 3.0 Å, whose intensity does not depend on the treatment temperature. Otherwise the intensities of the second peak (ca. 3.5 Å) increase with the thermal treatment. In order to understand this behavior, the second coordination shell had the structural parameters obtained as presented in Table 2. Fig. 4(B) presents the experimental and simulated curves. The best fit of the EXAFS data for the sample calcined at different temperatures was achieved when we assumed three-wave fitting for the simulation of this region, Nb–Nb, Nb–Si, and Nb–Nb. The theoretical phase shift and amplitude function used for the calculations of the structural parameters were extracted from Nb foil (ICSD file 76554) [20] and from $NbSi_2$ (ICSD file 16502) [21] compounds, also making use of the FEFF7.0 computational program. For pure Nb_2O_5, the fitting is satisfactory with only two distances with Nb–Nb lengths at 3.19 and 3.85 Å with a total coordination number around 6. Meanwhile for the sample, the best fit is achieved with three distances, two Nb–Nb lengths and an additional one for the Nb–Si length [32]. The samples calcined at 573 and 873 K present higher Nb–Nb distances compared to that obtained for the pure niobia, at 3.24 and 3.26 Å, and all the samples presented smaller coordination numbers, 1.0, 1.4, and 1.3, respectively. The coordination numbers related to the Nb–Si distances (3.39, 3.39, and 3.37 Å) do not change with increasing temperature, being maintained at 1.0, 1.0, and 1.4. Nevertheless, the coordination numbers related to the longer Nb–Nb distances (3.72, 3.76, and 3.69 Å) increase from 2.1 to 2.5 and 3.0, and are shorter than the presented by the pure niobia, when the sample is calcined at 573 and 873 K, respectively. Besides the presence of the two or three Nb–O lengths, the Nb–Si lengths also have been considered in the simulations for the second niobium coordination shell in Nb_2O_5/SiO_2 material. The shorter Nb–O distance has been associated to the Nb–O–Si linkage and the longer Nb–O distance to the Nb–O–Nb linkage [33,37].

3.3. Study of surface acidity

Fig. 5 shows the FT-IR spectra obtained for 2.5% Nb_2O_5/SiO_2, 5.0% Nb_2O_5/SiO_2 and 7.5% Nb_2O_5/SiO_2 samples after adsorption of pyridine followed by the thermal treatment at 383 K under low pressure ($\sim 10^{-5}$ Pa). The FT-IR spectra obtained, independent of the amount of Nb_2O_5 loading, present the same band positions, except for their intensities, which are slightly higher for matrices presenting higher amounts of the metal oxide. Thus, for estimation of the thermal stability of the acid sites only the vibrational spectra results for 2.5% Nb_2O_5/SiO_2 sample were considered.

Fig. 6 shows the FT-IR spectra obtained after adsorption of pyridine followed by heat treatment

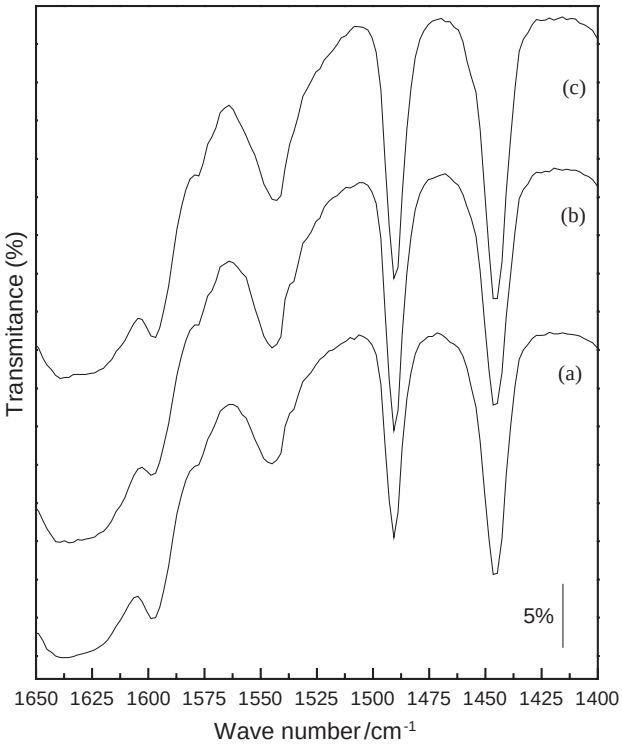

Fig. 5. FT-IR spectra of pyridine adsorbed on: (a) 2.5% Nb_2O_5/SiO_2; (b) 5.0% Nb_2O_5/SiO_2; and (c) 7.5% Nb_2O_5/SiO_2 samples under low pressure ($\sim 10^{-5}$ Pa for 30 min) at room temperature.

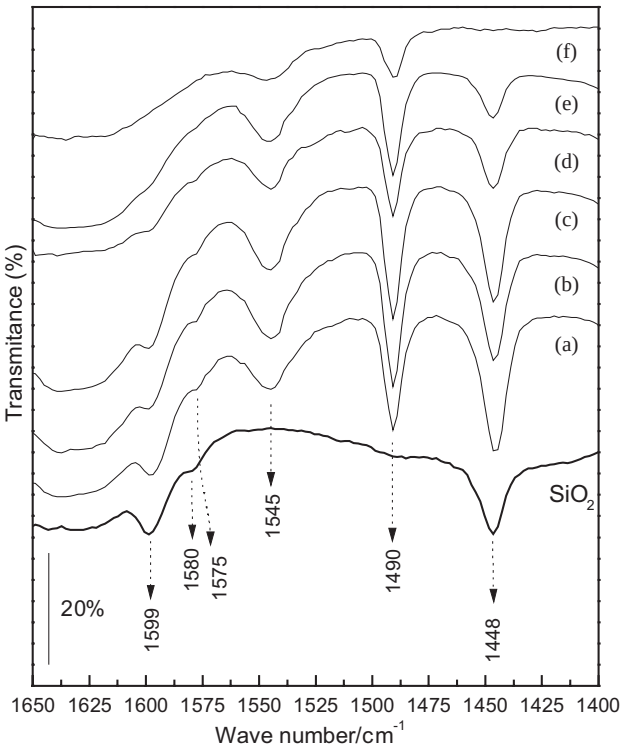

Fig. 6. FT-IR spectra of pyridine adsorbed on the 2.5% Nb_2O_5/SiO_2 sample under low pressure ($\sim 10^{-5}$ Pa for 30 min) at (a) room temperature, (b) 323 K, (c) 373 K, (d) 423 K, (e) 473 K, and (f) 523 K and on pure SiO_2 after the same treatment at room temperature.

between 298 and 523 K, under low pressure. For comparison, Fig. 6 also presents a spectrum of pure SiO_2 with adsorbed pyridine molecules submitted to $\sim 10^{-5}$ Pa at 298 K. The FT-IR spectra are limited in the wavenumber range between 1650 and 1400 cm^{-1}, where normal pyridine vibrational modes of interest are observed.

The bands at 1599 and 1448 cm^{-1} (Fig. 6(a)–(e)) are due to the 8*a* and 19*b* mode of pyridine bonded to the free silanol groups, ≡SiOH, through hydrogen bonding [37,38]. This band is also observed for pure SiO_2 treated at room temperature under 10^{-5} Pa.

The band observed at 1545 cm^{-1} for the samples heated between 298 and 523 K (Figs. 6(a)–(f)), is due to the 19*b* mode of pyridine molecules on a Brønsted acid site [10,39–41]. It is known that in pure Nb_2O_5 the Brønsted acid sites are thermally unstable at room temperature [42] but in the present case, for metal oxide in the sol–gel matrix, the thermal stability is considerably improved. This acid site is due to the OH groups attached to both groups, Nb–OH and also to Nb–OH–Si bridging [43], since for pure SiO_2 this band is not observed (Fig. 6). The Brønsted acid sites observed for the Nb_2O_5/SiO_2 system prepared by the grafting method and calcined at 473 K showed to be unstable with thermal treatment [44]. This acid site disappeared after drying at 373 K under low pressure.

The band observed at 1490 cm^{-1}, which does not disappear for the sample heated between 298 and 523 K (Fig. 6(a)–(f)), is due to the 19*a* mode and is always present for all kinds of pyridine adsorptions [38]. Physically adsorbed liquid-like pyridine 8*a* mode [10,45] is observed as a very weak band at 1580 cm^{-1} for SiO_2 and for the samples heated at 298 and 373 K (Fig. 6(a)–(c)).

The Lewis acid site, arising from coordinatively unsaturated Nb atom, was not observed. For Nb_2O_5 grafted on SiO_2 surface (a sub-monolayer of the metal oxide on the surface with the following characteristics: surface density of 1.7 Nb atoms per nm^2 and average Nb–Nb distance of 0.76 nm) the Lewis acid site is observed at 1450 cm^{-1} and is thermally stable up to 573 K [44]. It is possible that this band is overlapped with the 19*b* mode of pyridine bonded to free silanol groups through hydrogen bonding but on heating the sample at 523 K, no band assignable to pyridine adsorbed on a Lewis acid site is observed (Fig. 6(f)). The absence of Lewis acid sites is due to the method of preparation that produces niobium oxide particles with crystallite sizes about 7 nm [17]. In this case, the niobium atoms in the silica matrix are coordinatively saturated and, thus, no Lewis acid sites were detectable. It cannot be discarded the possibility that the physically sorbed water from the Lewis acid sites may not have been removed from the investigated materials calcined at 383 K, explaining why Lewis acid sites are not detected in the FT-IR studies.

4. Conclusions

The XPS study shows the existence of the metal in an ionic chemical environment formed in the Nb_2O_5/SiO_2 matrix during the sol–gel process and, probably, these species are related to Si–O–Nb bonds. The NbO_x structure in the matrix is very stable, since its local order is maintained under thermal treatment. We also could verify no change in Nb–Si length (from the second coordination sphere), confirming the good thermal stability of the Si–O–Nb linkages. On the other hand, the increase of the coordination number of the longest Nb–Nb and of the second peak from $|F(r)|$ with distances of 2.7–3.8 Å due to the thermal treatment, is related to less dispersion of the niobium species in the matrix (formation of niobium oxide agglomerates with significant size), leading to a decrease of the specific surface area [17]. At high temperatures, Nb_2O_5 amorphous particles crystallize into nanosized dimensions (6–21 nm) depending on the metal oxide amount in the sol–gel matrices. The thermal stability of Brønsted acid sites, Nb–OH and Nb–OH–Si groups, is due to the restricted mobility of the oxide particles imposed by Si–O–Nb bond formation in the sol–gel matrix.

Acknowledgments

This research work was partially performed at the LNLS—National Synchrotron Light Laboratory (LNLS), Brazil, XAS-Project 914/01. The authors wish to acknowledge Prof. Carol H. Collins (IQ-UNICAMP) for manuscript revision, Prof. Valmor R. Mastelaro (IFSC-USP) for discussion of the XAS results and Rita de C.G. Vinhas for technical assistance. M.S.P. Francisco is indebted to the São Paulo State Research Funding Foundation, FAPESP (Grant 01/01248-9) for a Postdoctoral fellowship.

References

[1] J.M. Jehng, I.E. Wachs, Catal. Today 8 (1990) 37.
[2] S.M. Maurer, E.I. Ko, J. Catal. 35 (1992) 125.
[3] I.E. Wachs, J.M. Jehng, G. Deo, H. Hu, N. Arora, Catal. Today 29 (1996) 1996.
[4] A. Yamaguchi, K. Asakura, Y. Iwasawa, J. Mol. Catal. A 146 (1999) 65.
[5] E.B. Pereira, M.M. Pereira, Y.L. Lam, C.A.C. Perez, M. Schmal, Appl. Catal. A 197 (2000) 99.
[6] M.M. Pereira, E.B. Pereira, L.Y. Lau, M. Schmal, Catal. Today 57 (2000) 291.
[7] X. Gao, I.E. Wachs, M.S. Wong, J.Y. Ying, J. Catal. 203 (2001) 18.

[8] Y.Z. Chen, B.J. Liaw, H.R. Tan, K.L. Shen, Appl. Catal. A 205 (2001) 61.
[9] K. Tanabe, Catal. Today 78 (2003) 65.
[10] J. Datka, A.M. Turek, J.M. Jehng, I.E. Wachs, J. Catal. 135 (1992) 186.
[11] J.M. Jehng, I.E. Wachs, Catal. Today 16 (1993) 417.
[12] Y. Gushikem, S.S. Rosatto, J. Braz. Chem. Soc. 12 (2001) 695.
[13] S.M. Maurer, D. Ng, E. Ko, Catal. Today 16 (1993) 319.
[14] S.M. Maurer, E.I. Ko, Catal. Lett. 12 (1992) 231.
[15] E.I. Ko, S.M. Maurer, J. Chem. Soc. (1990) 1062.
[16] H. Yoshida, T. Tanaka, T. Yoshida, T. Funabiki, Y. Yoshida, Catal. Today 28 (1996) 79.
[17] M.S.P. Francisco, Y. Gushikem, J. Mater. Chem. 14 (2002) 2514.
[18] J.H. Scofield, J. Electron Spectrosc. 89 (1976) 129.
[19] A. San-Miguel, Physica B 208 (1995) 177.
[20] B.M. Vasyutinski, G.N. Kartmazowy, Y.M. Smirnovy, V.A. Finkely, J. Less-Common Met. 87 (1982) 1.
[21] R. Kubiak, R. Horyny, H. Broday, K. Lukaszewiczy, Bull. Acad. Pol. Sci. 20 (1972) 429.
[22] C.D. Wagner, D.E. Passoja, H.F. Hillery, T.G. Kinisky, H.A. Sic, W.T. Jansen, J.A. Taylor, J. Vac. Sci. Technol. 21 (1982) 933.
[23] V.I. Nefedov, D. Gati, B.F. Dzhurinskii, N.P. Sergushin, Ya.V. Salyn, Russ. J. Inorg. Chem. 20 (1975) 1279.
[24] V. Pârvulescu, V.I. Pârvulescu, P. Grange, Catal. Today 57 (2000) 193.
[25] B.M. Reddy, I. Ganesh, E.P. Reddy, J. Phys. Chem. B 101 (1997) 1769.
[26] D. Briggs, M.P. Seah, Practical Surface Analysis, Vol. 1, 2nd Edition, Wiley, New York, 1993.
[27] V. Nazabal, E. Fargin, C. Labrugère, L. Flem, J. Non-Cryst. Solids 270 (2000) 223.
[28] J.F. Marco, J.R. Gancedo, F.J. Berry, Polyhedron 16 (1997) 2961.
[29] G.E. McGuire, G.K. Schweitzer, T.A. Carlson, Inorg. Chem. 12 (1973) 2450.
[30] S. Damyanova, L. Dimitrov, L. Petrov, P. Grange, Appl. Surf. Sci. 214 (2003) 68.
[31] L. Dragone, P. Moggi, G. Predieri, R. Zanoni, Appl. Surf. Sci. 187 (2002) 82.
[32] N. Ichikuni, Y. Iwasawa, Catal. Today 16 (1993) 427.
[33] K. Asakura, Y. Iwasawa, J. Phys. Chem. 95 (1991) 1711.
[34] G. Mosel, M. Willfahrt, U. Banach, Th. Hübert, J. Mater. Sci. 32 (1997) 1591.
[35] F. d'Acapito, S. Mobilio, P. Cikmacs, V. Merlo, I. Davoli, Surf. Sci. 468 (2000) 77.
[36] B.M. Gatehouse, A.D. Wadsley, Acta Crystallogr. 17 (1964) 1545.
[37] M. Nishimura, K. Asakura, Y. Iwasawa, J. Chem. Soc. (1986) 1660.
[38] E.P. Parry, J. Catal. 2 (1963) 371.
[39] E.V. Benvenutti, Y. Gushikem, C.U. Davanzo, S.C. de Castro, I.L. Torriani, J. Chem. Soc. Faraday Trans. 88 (1992) 3193.
[40] C. Morterra, G. Cerrato, Langmuir 6 (1990) 1810.
[41] M. Lefrancois, G. Malbois, J. Catal. 20 (1975) 350.
[42] Y. Inoue, H. Yamazaki, Y. Kimura, Bull. Chem. Soc. Jpn. 58 (1985) 2481.
[43] M.H. Zahedi-Niaki, S.M.J. Zaidi, S. Kaliaguine, Microp. Mesop. Mater. 32 (1999) 251.
[44] S. Denofre, Y. Gushikem, S.C. Castro, Y. Kawano, J. Chem. Soc. Faraday Trans. 89 (1993) 1057.
[45] G. Busca, Langmuir 2 (1986) 577.